Superior cyclic life of thermal barrier coatings with advanced bond coats on single-crystal superalloys

Authors: C.Vorkötter[A] ; D.E.Mack[A]; O.Guillon[A,B]; R.Vaßen[A]

Affiliations:

[A] Forschungszentrum Jülich GmbH, Institute of Energy and Climate Research, Materials Synthesis and Processing (IEK-1), 52425 Jülich, Germany

E-mail: c.vorkoetter@fz-juelich.de – Tel. +49 2461 61-96735;

d.e.mack@fz-juelich.de;

o.guillon@fz-juelich.de;

r.vassen@fz-juelich.de

[B] Jülich Aachen Research Alliance, JARA-Energy

Corresponding author: Christoph Vorkötter

Key words: thermal barrier coating, oxide dispersion strengthened, thermal spray, TGO, beta depletion

Abstract:

Advanced thermal barrier coatings are essential to further increase the efficiency of gas turbine engines. One limiting factor of the TBC lifetime is the temperature dependent formation of the thermally grown oxide (TGO) during thermal exposure resulting in critical stress levels at the top coat - bond coat interface. Oxide dispersion strengthened (ODS) bond coats demonstrated slower oxygen scale growth during thermal exposure in comparison to standard bond coats.

In this study for the first time TBC samples on single-crystal substrates (comparable to CMSX4) with thin ODS Co-based flash coats on the same Co-based bond coat (Amdry 995) and a porous atmospherically plasma sprayed (APS) yttria stabilized zirconia (YSZ) topcoat were manufactured by thermal spray techniques and evaluated with respect to their thermal cyclic behavior. As the major performance test cyclic burner rigs, which can establish thermal conditions similar to those in gas turbines, were applied.

TBC samples with the new material combination show superior performance compared to previous samples. Cross sections of the samples were analyzed by scanning electron and laser scanning microscopy. Lifetime data and failure mode of the samples are discussed with respect to material properties such as thermal expansion coefficients, microstructural changes and TGO growth.

1 Introduction

The energy conversion efficiency of a gas turbine rises with increasing combustion temperature. Higher combustion temperatures require high performance materials that resist the thermomechanical load in the gas turbine. Ni-based superalloys can resist temperatures up to 1050°C [1]. When the combustion temperature is further increased, thermal barrier coatings (TBCs) are commonly used to protect the superalloy against high temperature gases and oxidation. High performance TBCs allow to increase combustion temperature while maintaining the same lifetime of the gas turbine components.

A TBC often consists of a thermally sprayed ceramic top coat on a sprayed metallic bond coat. In most applications the superalloy components are air cooled from inside, with the ceramic top coat providing a significant temperature gradient through its low thermal conductivity. The bond coat's main purpose is to protect the underlying material from oxidation and to strengthen the bonding between top coat and substrate.

Common turbine blade materials are poly or single crystalline superalloys such as Inconel 738 and CMSX-4 [2]. For the first time, a promising advanced oxide dispersion strengthened bond coat material is associated with a single crystalline substrate and bond coat material, ERBO 1 and Amdry 995, to achieve higher TBC performance.

The lifetime of protective coatings is dependent on several parameters such as: mismatch of thermal expansion coefficients between different substrate materials and coating [3], microstructure especially porosity [4,5], bond coat roughness [6–9], operation temperature and related oxidation rates [10,11] and the surrounding atmosphere which might lead to corrosive attack by alkaline and sulphur or by silicates as CMAS [12]. A few relevant failure conditions are discussed in the following section.

The thermal expansion coefficient of the ceramic top coat is lower than that of the bond coat and the substrate. This mismatch leads to stresses during temperature changes. If the system is assumed stress free at room temperature, at high temperatures the top coat is under tensile

stress, which relaxes over time e.g. through creep processes. Subsequent cooling will lead to compressive stress in the top coat, which is often seen as major driving factor for coating spallation [7,13]. If the apparent energy release rate in the coating, mainly determined by the above-mentioned relaxation process and the stiffness of the top coat, approach the critical energy release rate, coating spallation will occur. Therefore a higher amount of stored energy is reducing the TBC lifetime.

Factors increasing the amount of stored energy in the top coat are e.g. a higher coating thickness, density and Young's modulus of the coating material. Phase transformations within the top coat, caused by the high temperatures at the coating surface, can result in additional stresses, leading to a higher amount of stored energy and a reduced lifetime, too.

The critical energy release rate, which is linked to the fracture toughness of the coating, should be as high as possible [14]. YSZ is often used as top coat material in TBCs [2,15].

For the bond coat different coating characteristics are important. The bond coat enhances the top coat's adhesion and protects the substrate from oxidation by forming a dense thermally grown oxide layer (TGO) between bond coat and top coat. The bonding of the ceramic top coat relies on a high roughness of the bond coat, which ensures a sufficient mechanical clamping as a major bonding mechanism. A dense and closed TGO layer is a diffusion barrier for oxygen reducing the oxidation rate, but further TGO growth reduces the bonding of the top coat, which finally leads to the failure of the coating, too. Thus the oxidation of the bond coat plays a major role for the coating lifetime.

The TGO growth is often divided up into three oxidation stages [16]. First the fast formation of a thin and dense oxide layer in case of MCrAlY (M= Co; Ni) coating an aluminum oxide scale forms. This scale protects the coating against further oxidation, which results in a slower oxidation rate. The following slower oxidation stage is the so called "steady stage" oxidation where the diffusion through the aluminum oxide scale is often the rate limiting step [17]. The

third “transient“ oxidation stage is the fast formation of mixed oxides followed by the spallation of the oxide layer/or the layer above.

The TGO introduces additional stresses in the TBC system due to its different material properties especially the low thermal expansion coefficient. This stress increases with higher TGO thickness and promotes crack propagation in the TGO and the top coat close to the TGO [7,18]. These cracks weaken the top coat- bond coat interface, or in a fracture mechanical approach reduce the critical energy release rate until the coating fails.

With a high bond coat roughness cracking and re-growing of the TGO is possible, prolonging the lifetime of the TBC system [19]. In this cracking mechanism the cracks are, as observed several times [19–22], formed initially at the peaks of the wavy bond coat-top coat interface caused by tensile stresses occurring by cooling down the “stress free” TBC system. Compressive stress states hinder the cracks to link from peak to peak. Finally, the low thermal expansion coefficient of the TGO leads to tensile stresses at the valley of the bond coat, causing crack linking and finally failure of the coating [18,19,23].

In previous studies, and although large scattering is evident, the logarithmic lifetime is proportional to the inverse bond coat temperature [10,11,19]. This proportionality is based on the diffusion induced TGO formation. The TGO is formed by diffusion of mainly aluminum but also reactive elements such as yttrium from the reservoir in the bond coat [24–26]. A critical TGO thickness leading to the failure of the TBC was reported by previous studies [10,19]. However, it appears that such critical TGO thicknesses are certainly dependent on the TBC system and also on the test conditions [27,28].

Due to the aluminum diffusion into the TGO, a beta depletion zone forms in the upper part of the bond coat. At a critical depletion the formation of transient oxides takes place, leading to the faster third stage of oxidation in the TGO [19,29,30]. This spinel formation was observed and related to the failure of the coating [31,32]. Depending on the material, the TGO growth rate may be enhanced by the additional formation of yttrium aluminates. The resulting lower

yttrium content in the bond coat may lead to a lower adhesion of the oxide scale and thus an early top coat delamination, too.

Additional thin flash coatings made of oxide dispersion strengthened material on top of the bond coat can reduce the TGO growth rate and result in a prolonged TBC lifetime [24,33,34]. Reasons for the slower scale growth are estimated to be the lower amount of yttrium aluminate precipitates in the oxide scale and coarser aluminum oxide scale grains, which reduce the oxide diffusion through the scale [24].

In a previous study on TBCs with oxide dispersion strengthened bond coats promising cycling results were achieved by using an advanced bond coat system with an additional thin oxide dispersion strengthened flash coat (40 µm Amdry 995, 2 % aluminum oxide) on a standard bond coat (120 µm Amdry 386) using Inconel 738 substrate [33].

Two materials are promising to achieve higher thermal cycling resistance. A Co-based bond coat (Amdry 995) shows a lower yttrium transport in comparison to a Ni-based one, leading to a longer TBC lifetime [26]. The single-crystal superalloy ERBO 1, which is comparable to CMSX-4, shows a lower thermal expansion coefficient than Inconel 738. A lower thermal expansion coefficient of the substrate leads to a lower amount of stored energy in the top coat after cooling and thus might prolong the cycling lifetime of the coating system.

Therefore a TBC system using those two materials can probably achieve higher thermal cycling performance. In this study for the first time the oxide dispersion strengthened TBC system is combined with the new material combination ERBO 1 substrate and Amdry 995 bond coat, discussing the failure modes and further reasons for the performance increase.

2 Material and methods

Four substrate bond coat material combinations were manufactured by thermal spraying, to evaluate the effect of oxide dispersion strengthened bond coats on the TBC lifetime with two different substrate/bond coat materials. A sample overview is presented in Table I**.** Detailed sample specifications are shown in Table II.

The first two characters of the sample name correspond to the material combination ER for ERBO 1 (comparable to CMSX-4) with Amdry995 bond coat and IN for Inconel 738 with Amdry 386 bond coat. The following three characters are "ODS" for samples with an additional ODS flash coat or "NON" for single layered bond coats. Samples with the same configuration are enumerated behind the characters.

For the ODS bond coat the oxide dispersion strengthened powders were produced by high energy milling in an attritor Simoloyer CM01 (ZoZ GmbH, Wenden, Germany) described in [35]. A milling run contained 120 g powder mixture, consisting of CoNiCrAlY alloy powder (Amdry 9954, Oerlicon Metco, Wholen, Switzerland) with 2 wt.% aluminum oxide powder (Martoxid MR70, Martinswerk, Bergheim, Germany) and 0.5 wt.% process control agent (stearic acid).A one liter steel milling chamber with 5 mm diameter steel balls was used with a powder to ball ratio of 1:10. During the 6 h milling run the milling speed was varied. One milling speed cycle was 1 min milling at 500 rpm and 4 min at 870 rpm to increase embedding of aluminum oxide. A milling run had 72 milling speed cycles. The powder of several milling runs was sieved to 36-56 µm to reduce the negative effects of a broad powder size distribution and to reduce the amount of e.g. elongated particles influencing the thermal spray process. Chemical analysis of the ODS powder, presented in Table III, were measured by inductive coupled plasma optical emission spectroscopy and combustion analysis. Chemical analysis results and SEM cross sections confirm the full embedding of aluminum oxide in irregular shaped particles.

The substrate material was cut by spark erosion to 30 mm in diameter and 3 mm thickness. To reduce the driving force for delamination at the edges these were rounded by machining. Before spraying samples were grit blasted which resulted in a relative constant substrate roughness of 2.73±0.22 µm R_a. The single-crystal superalloy ERBO-1 was developed within the SFB-Transregio 103 and was casted by the SFB-Transregio 103 service project Z01, which is located at Friedrich-Alexander Universität Erlangen-Nürnberg. Inconel 738 material was produced by Doncaster Precision Castings – Bochum GmbH (Germany). CTE measurements of the substrate materials were carried out with a 402 C (Netzsch, Germany) Dilatometer in Argon atmosphere.

The bond coat and the ODS flash coat were applied by vacuum plasma spraying (F4 gun Sulzer Metco, Wholen, Switzerland) to achieve highly dense coatings with a low oxide content, process parameters are listed in Table IV. To increase the adhesion of the bond coat the samples were diffusion annealed after spraying 4 h at 1140°C and 16 h at 870°C under argon atmosphere. The bond coat and substrate roughness of the samples were measured by a Cyberscan CT350 with a CHR1000 confocal white light sensor (cyberTECHNOLOGIES GmbH, Ingolstadt, Germany). Surface profiles were scanned in two perpendicular directions with a scan step size of 1 µm and divided up into single measurement parts according to DIN EN ISO 4288.

300-500 µm thick 8YSZ top coats were applied using 204NS (Oerlicon Metco,Wholen Switzerland) powder by atmospheric plasma spraying. Top coat layers were sprayed by a Multicoat facility (Oerlikon Metco, Wohlen, Switzerland) with a three-cathode TriplexPro$_{TM}$ 210 gun. Spraying parameters are presented in Table III. X-ray diffraction patterns of the top coat were measured by D4 Endeavour (Bruker AXS GmbH, Karlsruhe, Germany) with Cu-K_α radiation in theta to two theta mode.

To test the performance, all samples were thermally cycled in a burner rig facility until failure of the coating occurs [37]. Each cycle consists of five minutes heating by a natural gas oxygen flame followed by two minutes cooling by pressurized air. Coating failure was defined as at least 5 mm coating delamination and/or loss of the heat protection function indicated by significant deviation in the sample temperature. The surface temperature, measured by a pyrometer, was adjusted to 1400°C while the substrate temperature was kept constant at 1050°C or 1080°C measured by a thermocouple in the center of the sample. Bond coat temperatures were calculated by assuming one dimensional and homogeneous thermal conductivities of each layer [37]. The conductivities were assumed to be 1 W/(mK) for the top coat, 31 W/(mK) for the bond coat, and 26 W/(mK) for the substrate. Aging of the top coat is taken into account through assuming a slightly higher thermal conductivity for the top coat during high temperature exposure than in the as sprayed state [38]. The thermal conductivities for the ODS and non ODS bond coats were assumed to be equal, because of the low aluminum oxide concentration. For calculation of the bond coat temperature the measured layer thicknesses for each sample were used.

Cross sections of the samples were polished and analyzed by scanning electron microscope using a Phenom (Phenomworld B.V., Eindhoven, Netherlands) and a Ultra 55 (Carl Zeiss NTS GmbH, Oberkochen, Germany) SEM. For optical analysis a laser-scanning microscope (Keyence VK-9710, Neu-Isenburg, Germany) was used. The layer thickness was determined by using the average out of multiple SEM images. In each image the layer thickness was measured by AnalySIS (Olympus Soft imaging solutions GmbH*)* software with 20 measurement points per image. Porosity was evaluated through the contrast of pores and bulk material in SEM pictures by the use of AnalySIS. The errors correspond to the standard deviation of the mean values for each image.

3 Results and discussion

3.1 Thermal cycling results with new bond coat and substrate Amdry 995 and ERBO 1

In order to compare the performance of the different TBC samples, the bond coat temperature was taken into account. In Figure 1 the number of cycles to failure of the different TBC samples are plotted against the inverse bond coat temperature and the linear scale dependency of Vaßen et al. [10] is added to the graph. Reference TBC samples using Amdry 386 bond coat and Inconel 738 substrate were added to the graph marked by the triangles. Increased performance of the new reference samples compared to the old reference linear scale dependency is attributed to the now used higher porosity levels in the top coat.

By comparing the trendlines, samples with ERBO 1 substrate and Amdry 995 bond coat show a significant higher cycling performance in comparison to samples using Inconel 738 substrate and Amdry 386 bond coat. One reason for the performance increase is the lower thermal expansion coefficient mismatch. The CTE from 60-1080°C for the ERBO 1 substrate was measured to be about 12 % lower in comparison to the Inconel 738 one. Therefore the energy, available for the crack propagation and stored in the top coat after cooling the TBC system, is lower, resulting in a prolonged lifetime.

A second reason for the increased performance is a higher bond coat roughness providing a better mechanical clamping of the top coat. Previous studies show an increasing roughness by increasing the particle size distribution as well as a prolonged thermal cycling resistance especially for thick TBCs [8,9]. In Figure 2 the number of cycles to failure is plotted against the sample roughness. The D_{50} values of the used bond coat powders were added to the graph. The influence of the particle size distribution on the bond coat roughness is visible. Due to the different particle size the ERNON samples using Amdry 995 providing a higher surface roughness in comparison to INNON samples using Amdry 386 bond coat. As known from literature this might be a further reason for the increased coating lifetime [6,8,9].

The energy stored in the coating is affected by thickness and porosity of the top coat. The thicknesses and the porosities of the samples are presented in Table V. As discussed above one would expect decreasing cycling lifetime with increasing top coat thickness [5]. Our results show that the favourable CTE and the increase in roughness overweight this effect, with the result that the TBC samples with ERBO 1 and Amdry 995 have a higher cycling performance in comparison to the ones with Inconel 738 and Amdry 386.

A further explanation for the higher performance could be the lower yttrium diffusion in Amdry 995 in comparison to Amdry 386 [26] leading to a lower amount of yttrium aluminates in the TGO. The lower amount of yttrium aluminates in the TGO is visible in the two SEM images in the top row in Figure 3.

3.2 Superior lifetime by oxide dispersion strengthened bond coats.

By comparing the ODS and non ODS sample lifetimes the performance increase by the use of ODS bond coats is visible by comparison of filled and open symbols in Figure 1. The performance increase in comparison to the TBC samples without an additional ODS layer is visualized by the black arrows in Figure 1. TBC samples with the additional ODS layer using ERBO 1 substrate and Amdry 995 bond coat can reach numbers of cycles to failure about four times higher than TBC samples used in the reference [10] with Inconel 738 substrate and Amdry 386 bond coat. The different factors which can lead to the superior lifetime of the ODS samples are discussed in the following.

One reason for the higher performance of the ODS samples is the higher roughness of the ODS bond coat and the related increased adhesion of the top coat. In Figure 2 the number of cycles to failure is plotted against the roughness of the bond coat. By the use of ODS, the sample roughness increases. Samples with ODS bond coat show in average 25% higher roughness values for TBC samples using ERBO 1 and Amdry 995 and 32% higher roughness

for TBC samples using Inconel 738 and Amdry 386. A reason for the roughness increase is the coarser powder size distribution of the ODS powder.

A roughness increase for the ODS samples through bond coat rumpling is not assumable because of bad creep properties and increased hardness of the ODS bond coat.

By evaluating the number of cycles in respect to the roughness in Figure 2 an increase in the lifetime by increasing the bond coat roughness is visible, like in previous studies [6,8,9]. The roughness increase through the ODS seems to result in a higher cycling performance due to enhanced mechanical clamping of the top coat.

Besides the enhanced adhesion of the top coat the high roughness enables multiple cracking of the TGO, visible in case of samples using ERBO 1 substrate and Amdry 995 bond coat (see Figure 3). Thus tensile TGO growth stresses relax in multiple cracking of the thick TGO at the top of a wavy bond coat top coat interface avoiding cracks within the top coat as described by Naumenko et al [19]. This cracking and re-growing allows further TGO growth and results in TBC performance increase. Through the cracking of the TGO the protective scale locally decreases the oxidation protection. Therefore the oxidation rate might increase at these locations. Nevertheless through stress relaxation within the TGO the increased oxidation rate does not affect the TBC performance.

The performance increase through the use of the ODS is clearly visible for INODS and for ERODS samples. In case of the INODS sample the performance increase might be smaller, because the number of cycles to failure may be reduced by the formation of big pores at the bond coat/ODS bond coat interface. The formation of pores for the INODS sample, at the bond coat/ODS bond coat interface, visible in Figure 4, might occur due to the different base materials of ODS (Co - based) and bond coat (Ni -based) resulting in Kirkendall diffusion. The samples with ODS bond coats using ERBO 1 and Amdry 995 have the same base material for ODS and underlying bond coat and are not affected by pore formation at the bond coat/ODS bond coat.

Another reason for the lifetime increase is the higher oxidation resistance of the ODS bond coat, described in [24], resulting in a slower steady state oxidation and a delayed TGO induced failure. A further reason for the performance increase might be the ODS bond coat reducing the formation of yttrium aluminates in the TGO during the final stage of oxidation. In Figure 3 the SEM images of TBC samples using ODS bond coats, show a very low amount of yttrium aluminates in the TGO. This leads to the conclusion that the third stage oxidation is suppressed.

To determine lifetime the number of cycles to failure is plotted against the TGO thickness, see Figure 5. A critical TGO thickness leading to the failure of the coating could not be identified. As mentioned before a critical TGO thickness might not be visible due to influence of the TBC system through e.g. different top coat thickness and bond coat roughness.

The cycling samples with and without ODS show different beta depletion behavior. Figure 6 shows laser microscope images of the sample cross sections visualizing the beta depletion zones after thermal cycling. Using Amdry 995 instead of Amdry 386 bond coat the beta depletion zone at time of failure is several times larger. This is because of the lower aluminum content in Amdry 995 in comparison to Amdry 386 in combination with a higher lifetime/TGO thickness of those samples. Fully depleted bond coats may lead to an early failure of the sample [11,32]. Nevertheless in all samples the bond coats are not fully depleted, therefore further TGO growth and a higher number of cycles to failure, weather not suppressed by other failure inducing effects, is possible.

By a closer look on the extension of the beta depleted zone in each sample differences in the depletion behavior are visible. Depending on the material combination of the substrate and the bond coat one or two beta depletion zones are visible after thermal cycling. The lower beta depletion between the substrate and the bond coat is induced by the different aluminum concentrations of the bond coat and the substrate material. In case of the use of ERBO 1 and Amdry 995 the lower bond coat is forming an interdiffusion zone with the substrate, but no

depletion zone is visible. In this study, the bond coats are not fully depleted, so the lower depletion zone should not affect the aluminum reservoir used for the TGO formation, but may affect the diffusion of alloy elements by the different chemical composition.

In Figure 7 the TGO thickness is plotted against the thickness of the upper beta depletion zone for the different TBC samples after thermal cycling. The upper beta depletion zone between top coat and bond coat is mainly caused by diffusion of Al to the TGO, so the upper beta depletion zone for samples using IN738 and Amdry 386 without an ODS layer correlates linear with the TGO thickness, see Figure 7. In case of samples with an ODS layer the visible beta depletion zone occurs between ODS flash coat and bond coat. A depletion of the ODS material is assumable but not visible. The thickness of the upper beta depletion zone for the ODS coating samples is measured between ODS coating and bond coat.

Although the depletion of the ODS bond coat is not visible, the ODS bond coat can provide aluminum for the formation of the TGO. This was observed on an INODS sample with a low number of cycles to failure, showing a low TGO thickness and not (yet) visible beta depletion in the underlying standard ODS bond coat.

But the ODS bond coat seems to provide a reduced aluminum reservoir, since the beta depletion zone has the same thickness with approximately the same TGO thickness of non ODS and ODS bond coat (see Figure 7 sample ERODS3 and ERNON1).

In summary there are two main effects of the additional ODS bond coat leading to a performance increase. The first is the lower steady state oxidation rate, reduced due to the suppression of yttrium aluminate formation in the TGO and the suppression of the fast oxidation stage.

The second is the higher roughness of the ODS coatings, which ensures improved mechanical clamping of the top coat and allows stress reduction in the TGO by cracking and re-growing of the TGO.

3.3 Influence of YSZ top coat

Influences of the top coats on the cycling performance are discussed in the following. The failure mode of the samples indicate an oxidation induced failure resulting in a delamination at the TGO bond coat/ top coat interface. All samples show a similar delamination at the TGO as an example cross section of sample ERODS2 is shown in Figure 8. The delamination of the top coat is visible within the TGO and partially slightly above the TGO (Figure 8). In the bottom right and top left hand corner of Figure 3 examples for the cracks within the TGO are visible. The top coat that was still connected to the bond coat shows no cracks reaching from the surface to the bond coat, so the top coat seems to stay intact until delamination at the TGO during cracking and re-growing of the TGO occurs. As a result of TGO delamination the samples show mainly edge delamination of the top coat with a blue oxidized bond coat underneath, see Figure 9.

In TBC samples the phase transition of the top coat to the monoclinic phase with a significant higher density in comparison to the monoclinic and cubic phase, would induce changes in the local density of the top coat. Densification can induce additional stresses in the top coat, which may lead to an early failure of the coating. Previous studies show that the monoclinic phase in the top coat material occurs at reduced cooling rates of the samples [39]. The XRD diffraction pattern of sample ERODS1, presented in Figure 10, shows no visible monoclinic phase, even after a high number of cycles (3300). The samples surface contains cubic and tetragonal phase but no monoclinic phase. Drawn from the phase composition stresses leading to an early top coat failure due to phase transitions were excluded. The cooling by pressurized air seems to be fast enough to disable the monoclinic phase transformation of the top coat material.

Sintering at high temperatures during the thermal cycling can result in a larger amount of stored energy in the coating, leading to a fast delamination of the TBC. Sintering effects in the top coat are visible up to high cycling lifetimes. In Figure 11 the top coat porosities for

different TBC samples are presented in respect to the number of cycles to failure. The porosity of a non-cycled ERODS sample was added. For the ERODS samples reaching high number of cycles to failure sintering effects are visible. The porosity for the TBC samples using ERBO 1 and Amdry 995 and an additional bond coat decreases by a maximum of 36 % after 4200 cycles. A dense coating increases the amount of energy stored in the top coat after cooling. Therefore a reduced number of cycles to failure of these samples through sintering could not be excluded, but vice versa this underlines the good bond coat properties of these samples providing a good adhesion reaching high number of cycles to failure even with lower top coat porosity. Top coat sintering of the other samples showing lower number of cycles to failure is not clearly visible.

4 Conclusion

Thin oxide dispersion strengthened flash coats nearly double the lifetime of the TBC sample in comparison to single layered bond coats. The double layered bond coat ODS samples result in a high thermal cycling resistance reaching more than 4000 cycles at 1400°C top coat and 1080 °C bond coat temperature. The bond coat oxidation could be identified as the lifetime limiting factor.

Reasons for the increased thermal cycling performance by the ODS flash coat could be attributed to:

- Suppression of the yttrium aluminate formation in the TGO (known as overdoping effect) and positive influence on the alumina scale grain boundary oxygen diffusion leading to a higher oxidation resistance of the ODS material.
- Better adhesion of the top coat and multiple cracking of the TGO enabling stress relaxation and avoiding failure of the top coat, as a result of higher ODS bond coat roughness.

5 Acknowledgements

This work was funded by SFB Transregio 103 (Project number B6). We thank our cooperation partners for the supply of the single-crystal superalloy material. The authors acknowledge the contribution of the following colleagues in our Institute:
Dr. Jan Bergholz for providing the INODS samples, Mr. Ralf Laufs, Mr. Frank Kurze and Mr. Karl-Heinz Rauwald for the invaluable assistance during plasma spraying and Mr. Martin Tandler for the effort with the cyclic burner rig tests. We also would like to thank Dr. Doris Sebold for SEM analysis and assistance and our colleagues at ZEA-3, Forschungszentrum Jülich, Germany, who performed the chemical analysis.

References

[1] T.M. Pollock, S. Tin, Nickel-Based Superalloys for Advanced Turbine Engines, Journal of Propulsion and Power 22 (2006) 361–374.

[2] R.C. Reed, The superalloys: Fundamentals and applications, Cambridge University Press, Cambridge, 2006.

[3] X. Li, X. Huang, Q. Yang, Z. Tang, Effects of substrate material and TBC structure on the cyclic oxidation resistance of TBC systems, Surface and Coatings Technology 258 (2014) 49–61.

[4] E. Bakan, D.E. Mack, G. Mauer, R. Vaßen, T. Troczynski, Gadolinium Zirconate/YSZ Thermal Barrier Coatings, J. Am. Ceram. Soc. 97 (2014) 4045–4051.

[5] M.A. Helminiak, N.M. Yanar, F.S. Pettit, T.A. Taylor, G.H. Meier, Factors affecting the microstructural stability and durability of thermal barrier coatings fabricated by air plasma spraying, Materials and Corrosion 63 (2012) 929–939.

[6] R. Eriksson, S. Sjöström, H. Brodin, S. Johansson, L. Östergren, X.-H. Li, TBC bond coat–top coat interface roughness, Surface and Coatings Technology 236 (2013) 230–238.

[7] R. Vaßen, G. Kerkhoff, D. Stöver, Development of a micromechanical life prediction model for plasma sprayed thermal barrier coatings, Materials Science and Engineering: A 303 (2001) 100–109.

[8] K. Yuan, Y. Yu, J.-F. Wen, A study on the thermal cyclic behavior of thermal barrier coatings with different MCrAlY roughness, Vacuum 137 (2017) 72–80.

[9] F. Traeger, M. Ahrens, R. Vaßen, D. Stöver, A life time model for ceramic thermal barrier coatings, Materials Science and Engineering: A 358 (2003) 255–265.

[10] R. Vaßen, S. Giesen, D. Stöver, Lifetime of Plasma-Sprayed Thermal Barrier Coatings, J Therm Spray Tech 18 (2009) 835–845.

[11] S. Rezanka, Abscheidung von Wärmedämmschichtsystemen mit dem Plasma Spray-Physical Vapor Deposition- (PS-PVD-) Prozess - Untersuchung des Prozesses und der hergestellten Schichten. Dissertation, 2015.

[12] C. Jiang, E.H. Jordan, A.B. Harris, M. Gell, J. Roth, Double-Layer Gadolinium Zirconate/Yttria-Stabilized Zirconia Thermal Barrier Coatings Deposited by the Solution Precursor Plasma Spray Process, J Therm Spray Tech 24 (2015) 895–906.

[13] M. Ahrens, S. Lampenscherf, R. Vaßen, D. Stöver, Sintering and Creep Processes in Plasma-Sprayed Thermal Barrier Coatings, Journal of Thermal Spray Technology 13 (2004) 432–442.

[14] J.F. Knott, Fundamentals of fracture mechanics, Pe Men Book Co, Taipei, 1981.

[15] E. Bakan, R. Vaßen, Ceramic Top Coats of Plasma-Sprayed Thermal Barrier Coatings, J Therm Spray Tech 26 (2017) 992–1010.

[16] H. Hindam, D.P. Whittle, Microstructure, adhesion and growth kinetics of protective scales on metals and alloys, Oxid Met 18 (1982) 245–284.

[17] D.J. Young, High temperature oxidation and corrosion of metals: David J. Young, Elsevier, Amsterdam, Oxford, Cambridge, 2016.

[18] C. Nordhorn, R. Mücke, R. Vaßen, Simulation of the effect of realistic surface textures on thermally induced topcoat stress fields by two-dimensional interface functions, Surface and Coatings Technology 258 (2014) 181–188.

[19] D. Naumenko, V. Shemet, L. Singheiser, W.J. Quadakkers, Failure mechanisms of thermal barrier coatings on MCrAlY-type bondcoats associated with the formation of the thermally grown oxide, J Mater Sci 44 (2009) 1687–1703.

[20] K. Schlichting, N. Padture, E. Jordan, M. Gell, Failure modes in plasma-sprayed thermal barrier coatings, Materials Science and Engineering: A 342 (2003) 120–130.

[21] W. Nowak, D. Naumenko, G. Mor, F. Mor, D.E. Mack, R. Vassen, L. Singheiser, W.J. Quadakkers, Effect of processing parameters on MCrAlY bondcoat roughness and lifetime of APS–TBC systems, Surface and Coatings Technology 260 (2014) 82–89.

[22] N.P. Padture, M. Gell, E.H. Jordan, Thermal barrier coatings for gas-turbine engine applications, Science (New York, N.Y.) 296 (2002) 280–284.

[23] C. Nordhorn, R. Mücke, D.E. Mack, R. Vaßen, Probabilistic lifetime model for atmospherically plasma sprayed thermal barrier coating systems, Mechanics of Materials 93 (2016) 199–208.

[24] T. Huang, J. Bergholz, G. Mauer, R. Vassen, D. Naumenko, W.J. Quadakkers, Effect of test atmosphere composition on high-temperature oxidation behaviour of CoNiCrAlY coatings produced from conventional and ODS powders, Materials at High Temperatures 2 (2017) 1–11.

[25] A. Gil, V. Shemet, R. Vassen, M. Subanovic, J. Toscano, D. Naumenko, L. Singheiser, W.J. Quadakkers, Effect of surface condition on the oxidation behaviour of MCrAlY coatings, Surface and Coatings Technology 201 (2006) 3824–3828.

[26] J. Toscano, R. Vaβen, A. Gil, M. Subanovic, D. Naumenko, L. Singheiser, W.J. Quadakkers, Parameters affecting TGO growth and adherence on MCrAlY-bond coats for TBC's, Surface and Coatings Technology 201 (2006) 3906–3910.

[27] C.-J. Li, H. Dong, H. Ding, G.-J. Yang, C.-X. Li, The Correlation of the TBC Lifetimes in Burner Cycling Test with Thermal Gradient and Furnace Isothermal Cycling Test by TGO Effects, J Therm Spray Tech 26 (2017) 378–387.

[28] H. Zhao, Z. Yu, H.N. Wadley, The influence of coating compliance on the delamination of thermal barrier coatings, Surface and Coatings Technology 204 (2010) 2432–2441.

[29] Philipp J. Terberger, Alterung von Vakuum-plasmagespritzten MCrAlY-Schutzschichten und ihre Wechselwirkung mit Nickel- und Cobalt y-y' mbasierten Superlegierungen. Dissertation, 2015.

[30] A. Rabiei, Failure mechanisms associated with the thermally grown oxide in plasma-sprayed thermal barrier coatings, Acta Materialia 48 (2000) 3963–3976.

[31] A. Gil, D. Naumenko, R. Vassen, J. Toscano, M. Subanovic, L. Singheiser, W.J. Quadakkers, Y-rich oxide distribution in plasma sprayed MCrAlY-coatings studied by SEM with a cathodoluminescence detector and Raman spectroscopy, Surface and Coatings Technology 204 (2009) 531–538.

[32] S. Rezanka, G. Mauer, R. Vaßen, Improved Thermal Cycling Durability of Thermal Barrier Coatings Manufactured by PS-PVD, J Therm Spray Tech 23 (2014) 182–189.

[33] Jan Bergholz, Herstellung und Charakterisierung oxiddispersionsverstärkter Haftvermittlerschichten, Dissertation, 2016.

[34] K.A. Unocic, J. Bergholz, T. Huang, D. Naumenko, B.A. Pint, R. Vaßen, W.J. Quadakkers, High-temperature behavior of oxide dispersion strengthening CoNiCrAlY, Materials at High Temperatures 35 (2017) 108–119.

[35] J. Bergholz, B.A. Pint, K.A. Unocic, R. Vaßen, Fabrication of Oxide Dispersion Strengthened Bond Coats with Low Al2O3 Content, J Therm Spray Tech 26 (2017) 868–879.

[36] M.J. Donachie, S.J. Donachie, Superalloys: A technical guide, 2nd ed., ASM International, Materials Park OH, 2002.

[37] F. Traeger, R. Vaßen, K.-H. Rauwald, D. Stöver, Thermal Cycling Setup for Testing Thermal Barrier Coatings, Adv. Eng. Mater. 5 (2003) 429–432.

[38] H.-J. Rätzer-Scheibe, U. Schulz, The effects of heat treatment and gas atmosphere on the thermal conductivity of APS and EB-PVD PYSZ thermal barrier coatings, Surface and Coatings Technology 201 (2007) 7880–7888.

[39] J. Moon, H. Choi, H. Kim, C. Lee, The effects of heat treatment on the phase transformation behavior of plasma-sprayed stabilized ZrO2 coatings, Surface and Coatings Technology 155 (2002) 1–10.

Table I Sample overview.

Sample	INNON	INODS	ERNON	ERODS
Substrate	Inconel 738	Inconel 738	ERBO 1	ERBO 1
Bond coat	Amdry 386	Amdry 386	Amdry 995	Amdry 995
ODS bond coat	n.a.	Amdry 995 2% Al_2O_3	n.a.	Amdry 995 2% Al_2O_3

Table II Specifications of samples after thermal cycling (roughness measured before).

Sample (internal number)	Cycles to failure	TGO thickness [µm]	ODS bond coat thickness [µm]	Upper beta depletion zone thickness TGO-BC [µm]	Lower beta depletion zone thickness ;BC-substrate [µm]	Standard bond coat thickness [µm]	R_a bond coat [µm]	Bond coat temperature [°C]
ERODS1 (4214)	3300	11.4±1.9	44±4	59±9	n.a.	126±6	9.9	1077
ERODS2 (4215)	4249	11.8±2.1	43±4	44±9	n.a.	162±4	10.2	1082
ERODS3 (4213)	1899	7.7±1.3	45±6	55±13	n.a.	147±7	9.9	1108
INODS (2048)	1445	5.1±1.0	55±7	19.9±2.8	22.1±1.4	111±8	8.3	1100
ERNON1 (4310)	2294	7.5±1.0	n.a.	56±3	n.a.	238±4	9.4	1086
ERNON2 (4309)	1637	7.6±2.6	n.a.	83±7	n.a.	170±8	9.4	1108
INNON1 (3644)	1221	10.9±1.7	n.a.	27.1±1.6	20.1±0.8	134±6	7.0	1090
INNON2 (3627)	1284	9.3±1.2	n.a.	25±0.6	22.1±2.1	125±6	6.5	1091
INNON3 (3628)	985	8.2±0.7	n.a.	22.4±1.2	23.6±1.4	132±6	6.5	1089

Table III Chemical compositions in weight percent taken from [29,33,36] chemical analysis of the ODS powder measured by inductive coupled plasma optical emission spectroscopy and combustion analysis. Size distribution measured by laser diffraction with a Horiba LA-950 (Horiba Ltd, Kyoto, Japan).

Material	Ni	Co	Cr	W	Re	Mo	Al	Ti	Ta	Hf	C	Y	O	D_{10} [µm]	D_{50} [µm]	D_{90} [µm]
ERBO1	Bal	9	6.5	6	3	0.6	5.6	1	6.5	-	0.01		-	-	-	-
Inconel 738	61.5	8.5	16	2.6		1.75	3.4	3.4	1.75	-	0.17		-	-	-	-
Amdry 995	34	Bal	21.3	-	-	-	8.39	-	-	-	-	0.42	-	21	32	49
Amdry 386	Bal	22.2	16.7		-	-	13	-	-	0.29	-	0.61	-	16	24	37
ODS Powder	31.5	37.7	20.8	0.04	-	-	8.7	-	0.01	-	0.32	0.46	1.13	32	48	72

Table IV Process parameters for thermal spray.

System	Plasma Torch	Current [A]	Voltage [V]	Ar/H [slpm]	Feeding Gas Ar [slpm]	Powder feeder	Pressure	Distance [mm]	Robot Speed [mm/s]
VPS	F4	640 /680 (ODS)	70	50/9	1.7	15 %	60 mbar	275	440
APS	Triplex Pro 210TM	420	90	46/0	2	20 %	1 atm	200	500

Table V Sample porosities and layer thicknesses.

Sample	ERODS1	ERODS2	ERODS3	INODS	ERNON1	ERNON2	INNON1	INNON2	INNON3
Cycles to failure	3300	4249	1899	1445	2294	1637	1221	1284	985
Top coat thickness [µm]	533±8	511±6	507±12	324±14	534±6	578±6	405±26	400±50	386±24
Top coat porosity [%]	12.3±0.9	9.9±1.3	13.4±1.5	16.9±1.9	19.5±1.8	15.1±1.4	16.3±1.7		

List of figure captions:

Figure 1 Arrhenius plot of the cycles to failure and the bond coat temperature for YSZ top coat TBCs with different bond coats. Samples tested at 1400°C top coat temperature, linear dependency - black line - taken from [10], INODS sample taken from [33]. TBC samples from current investigation using ERBO 1 and Amdry 995 are marked by rectangles, using Inconel 738 and Amdry386 by triangles. Not filled data points are referring to single layered bond coat TBC samples, filled ones to double layered ODS bond coats. The linear scale dependency is used to set the approximate performance trendlines of the INNON - grey - and the ERNON samples - black - , marked by dashed lines. Increases in performance are visible for ODS samples marked by arrows.

Figure 2 Number of cycles to failure vs. bond coat roughness for different TBC samples after thermal cycling showing in average 42 % higher roughness for the Amdry 995 bond coat and increased roughness values for ODS bond coat.

Figure 3 SEM cross-sections of the TGO for different TBC samples after thermal cycling. A cracked and re-grown TGO in an ODS sample at regions where the top coat is still attached is visible in bottom right hand corner. Reduced amount of yttrium aluminates in the TGO is visible for Co-based Amdry 995 sample. Further reduced amount of yttrium aluminates is visible for ODS bond coats.

Figure 4 SEM cross sections of the double layered ODS bond coat for two different samples after thermal cycling. For the sample with a ODS bond coat using IN738 and Amdry 386 pores within the ODS are visible.

Figure 5 Number of cycles to failure vs. TGO thickness for different TBC samples after thermal cycling.

Figure 6 Laser scanning microscope images of three different TBC system cross sections after thermal cycling showing one or two beta depletion zones depending on the bond coat material.

Figure 7 Plot of the TGO thickness vs. upper depletion zone thickness for different TBC samples after thermal cycling. Samples with ODS bond coat ERODS3 show the same beta depletion zone and TGO thickness as non ODS samples ERNON1 indicating a lower Al reservoir in the ODS bond coat. A linear dependency of the upper depletion zone thickness to the TGO thickness is visible for INNON samples.

Figure 8 SEM cross section of sample ERODS2 showing YSZ delamination at TGO, cracks within the TGO after 4249 cycles at 1400°C.

Figure 9 Top view of the TBC samples after thermal cycling showing edge delamination as main failure.

Figure 10 XRD diffraction pattern of as sprayed (reference sample) and thermally cycled ERODS1 YSZ top coat

Figure 11 Top coat porosity against cycles to failure of the samples for different TBC samples, reference sample without thermal cycling and trendline for ERODS samples was added, showing the sintering in the top coat.

Figures:

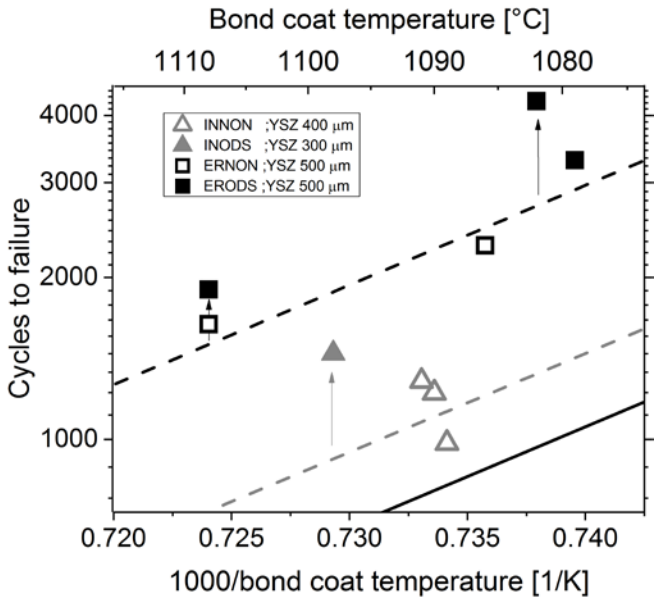
Bond coat temperature [°C]
1110
1100
1090
1080
4000
3000
2000
1000
Cycles to failure
INNON ;YSZ 400 µm
INODS ;YSZ 300 µm
ERNON ;YSZ 500 µm
ERODS ;YSZ 500 µm
0.720
0.725
0.730
0.735
0.740
1000/bond coat temperature [1/K]

1

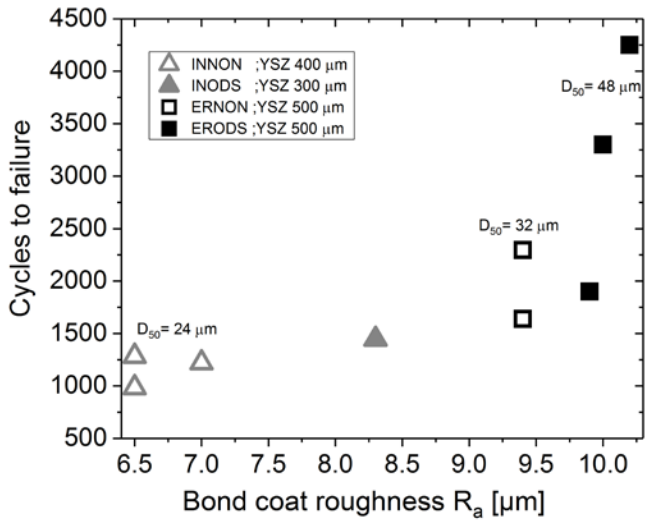
4500
4000
3500
3000
2500
2000
1500
1000
500
Cycles to failure
INNON ;YSZ 400 µm
INODS ;YSZ 300 µm
ERNON ;YSZ 500 µm
ERODS ;YSZ 500 µm
D50= 48 µm
D50= 32 µm
D50= 24 µm
6.5
7.0
7.5
8.0
8.5
9.0
9.5
10.0
Bond coat roughness Ra [µm]

2

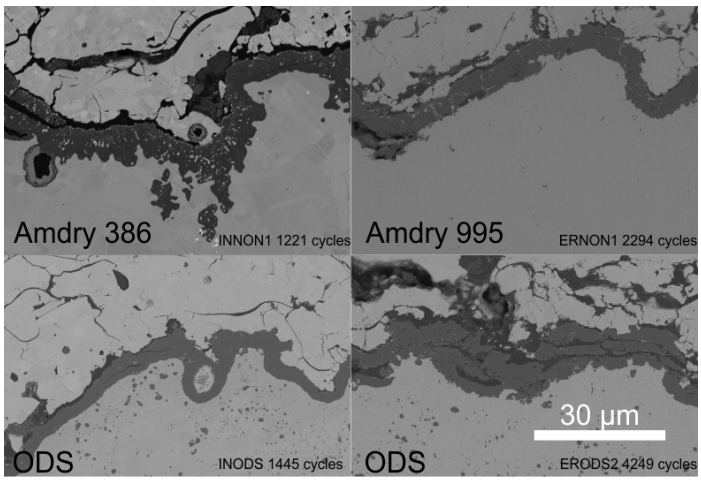
Amdry 386
INNON1 1221 cycles
Amdry 995
ERNON1 2294 cycles
ODS
INODS 1445 cycles
ODS
ERODS2 4249 cycles
30 µm

3

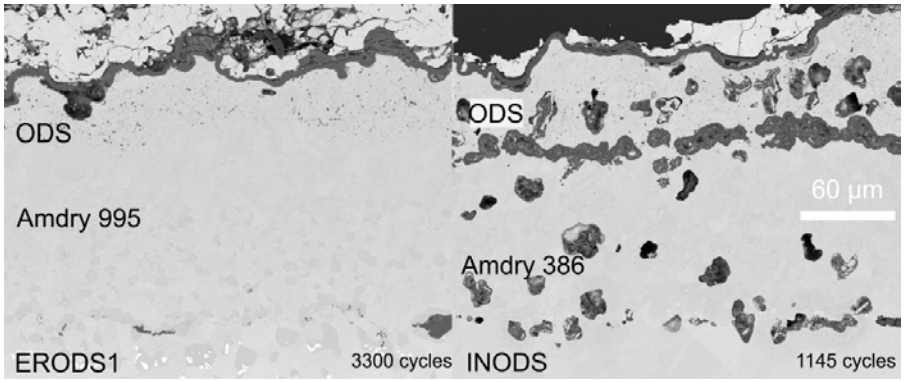
ODS
Amdry 995
ERODS1
3300 cycles
ODS
Amdry 386
INODS
1145 cycles
60 µm

4

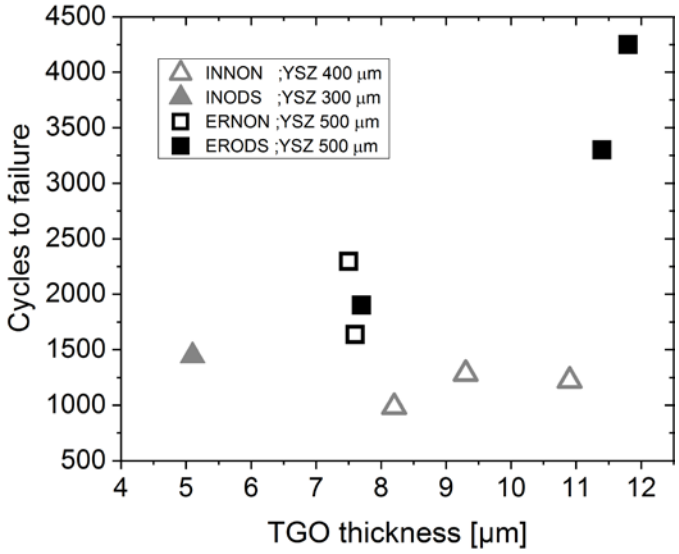
INNON ;YSZ 400 µm
INODS ;YSZ 300 µm
ERNON ;YSZ 500 µm
ERODS ;YSZ 500 µm
Cycles to failure
TGO thickness [µm]
4500
4000
3500
3000
2500
2000
1500
1000
500
4
5
6
7
8
9
10
11
12

5

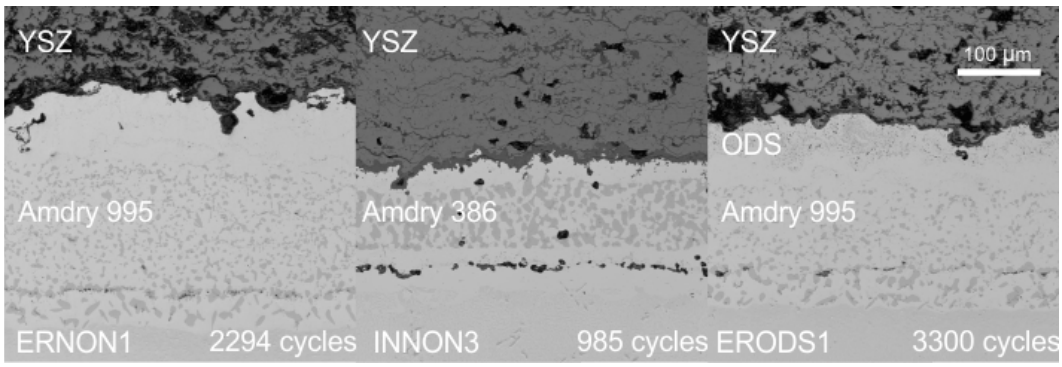
YSZ
YSZ
YSZ
100 µm
ODS
Amdry 995
Amdry 386
Amdry 995
ERNON1
2294 cycles
INNON3
985 cycles
ERODS1
3300 cycles

6

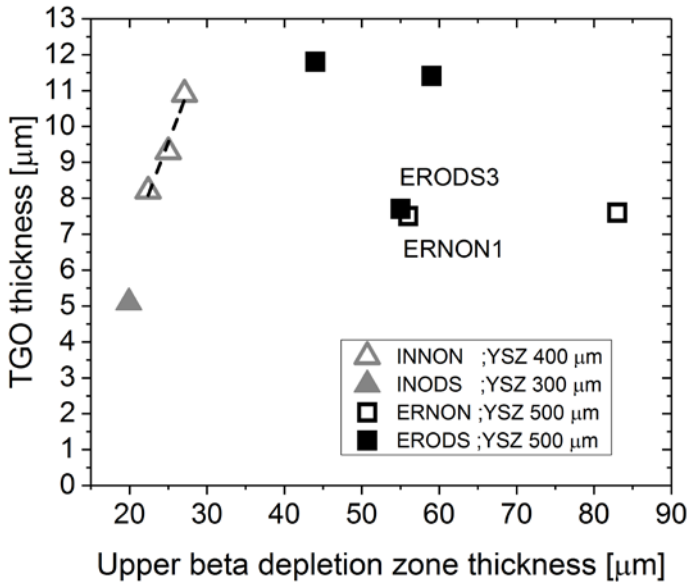
TGO thickness [µm]
Upper beta depletion zone thickness [µm]
ERODS3
ERNON1
INNON ;YSZ 400 µm
INODS ;YSZ 300 µm
ERNON ;YSZ 500 µm
ERODS ;YSZ 500 µm

7

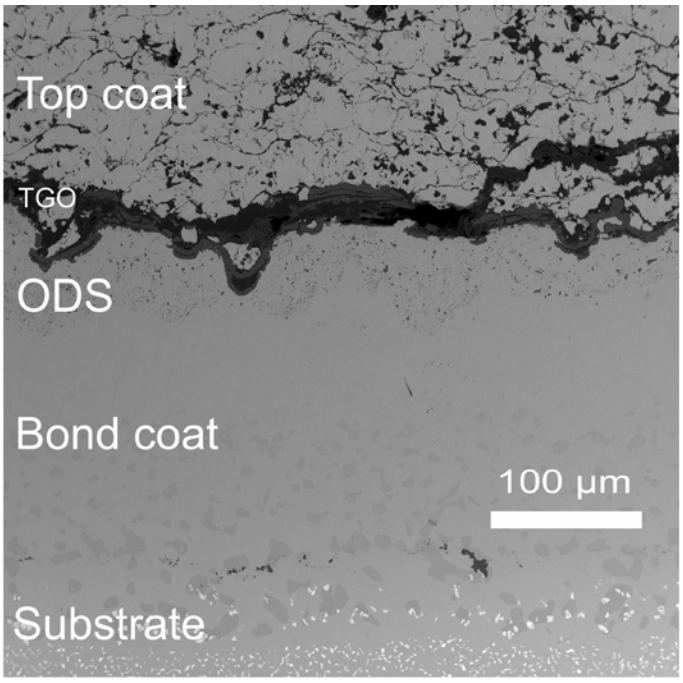
Top coat
TGO
ODS
Bond coat
100 µm
Substrate

8


ERODS1
ERODS2
ERODS2
ERNON1
ERNON2
INODS1
INNON1
INNON2
INNON3

9

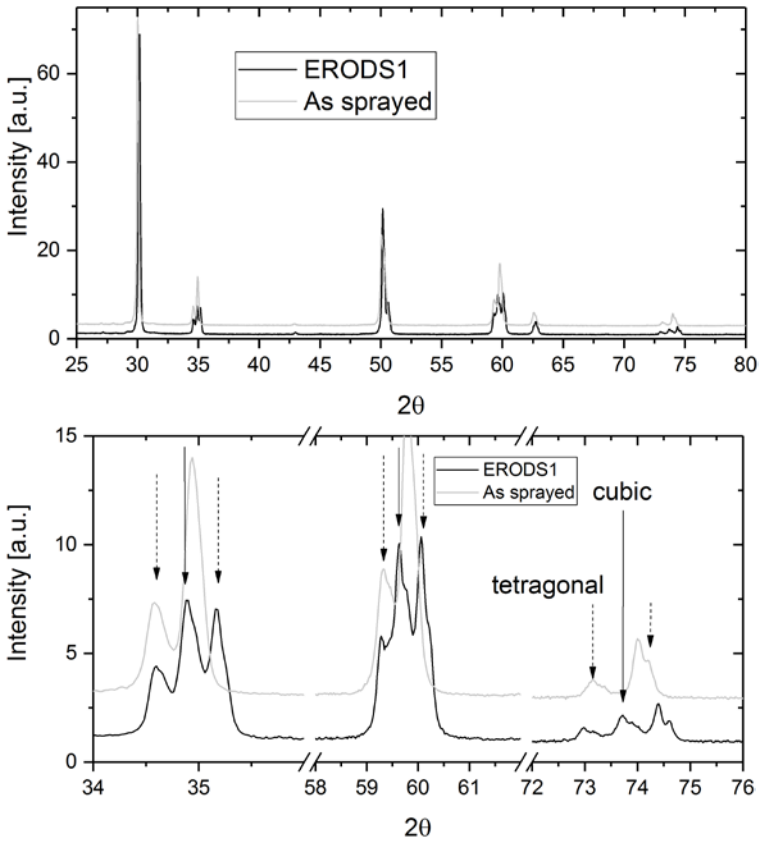
ERODS1
As sprayed
Intensity [a.u.]
2θ
ERODS1
As sprayed
cubic
tetragonal
Intensity [a.u.]
2θ

10

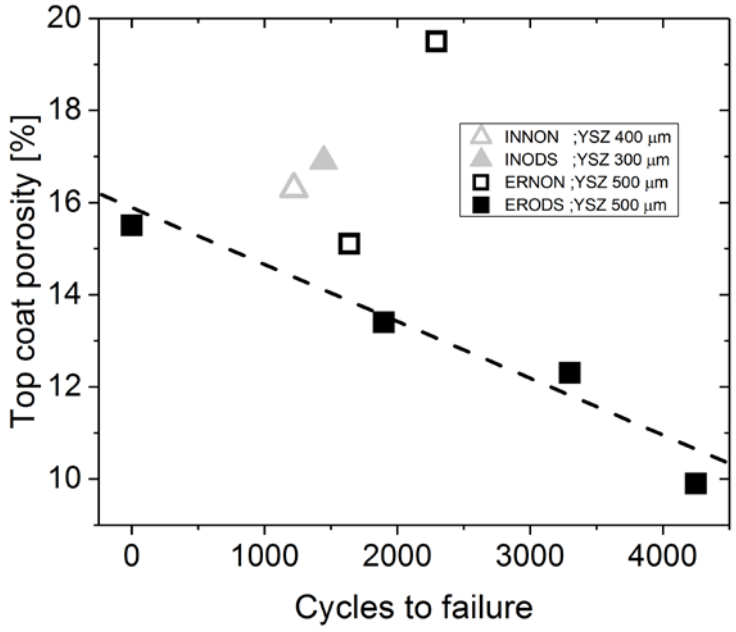
Top coat porosity [%]
Cycles to failure
INNON ;YSZ 400 μm
INODS ;YSZ 300 μm
ERNON ;YSZ 500 μm
ERODS ;YSZ 500 μm
20
18
16
14
12
10
0
1000
2000
3000
4000

11